

Study of Compressed Log-Periodic Dipole Antennas

COLIN C. BANTIN, MEMBER, IEEE, AND KEITH G. BALMAIN, MEMBER, IEEE

Abstract—The behavior of log-periodic dipole (LPD) antennas, which are compressed along the transmission-line axis, is studied both experimentally and theoretically. Compressed LPD antennas are found to be efficient, of low gain, and frequency independent. With compression, the radiation pattern approaches dipole-like behavior and the bandwidth increases slightly. It is also found that LPD antennas exhibit anomalous frequency-dependent behavior in narrow bands of frequencies ($\approx 1/8$ of a log period in width) when a reactive termination is used and when the scaling factor τ is below about 0.92–0.93.

INTRODUCTION

THE general behavior of the basic log-periodic dipole (LPD) antenna is well known [1], [2]. Recent work has been devoted to reducing the size of the array by using shortened helical elements [3], [4] and by capacitive and inductive loading [5]. A more accurate method of analysis has been introduced, using an approximate three-term current distribution [6], and there are more recent efforts to circumvent the necessity of feeder transposition [7]. In general, the parameters used for LPD models tend toward values appropriate for high gain (large τ and σ and small α , see Fig. 1) but there has been no published work on antennas compressed along the transmission-line axis other than the results of Carrel [2] whose values of σ or α do not go below 0.05 or above 30° , respectively. The purpose of this paper is to examine the behavior of LPD arrays compressed in this manner to high values of α resulting in closely spaced elements. There are three main areas of investigation:

- 1) properties of individual LPD antennas over the design bandwidth, including radiation patterns, input impedance, and operating bandwidth;
- 2) properties of sequences of LPD antennas at a constant midband frequency, including power gain, directivity, efficiency, radiation patterns, and input impedance;
- 3) anomalous frequency-dependent behavior consisting of beam-splitting and high back-lobe levels occurring over very narrow bands of frequencies.

Experimental results are presented for two constant- τ sequences of LPD antenna models and compared with theoretical results based on the sinusoidal current-distribution approximation for the elements. Calculated results are

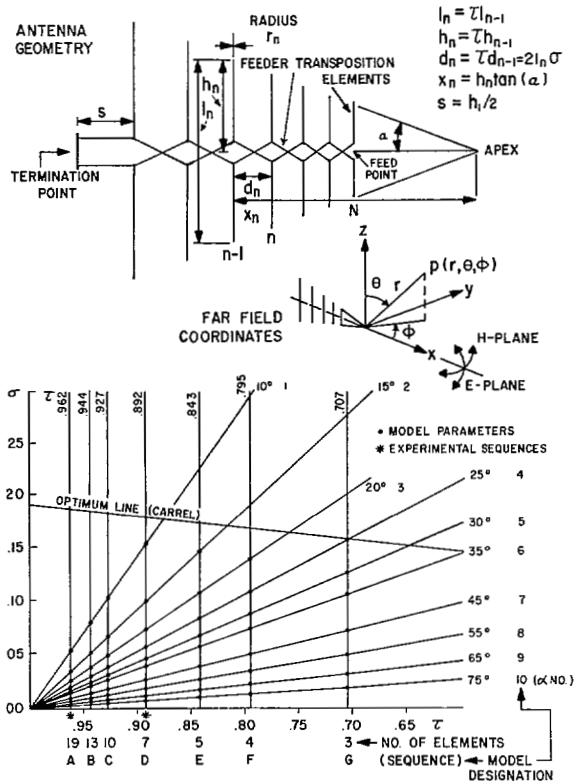


Fig. 1. Basic LPD parameters, test parameters, and sequence numbering; termination Z_t = short circuit or matched; structure bandwidth = $h_i/h_N = 2:1$; unloaded feeder impedance $Z_0 = 100$ ohms; half-length to radius ratio = $h_i/r_i = 145$ (for all models).

also presented for other constant- τ sequences to define the various trends more completely over the range of parameters indicated in Fig. 1.

THEORETICAL CALCULATIONS AND EXPERIMENTAL PROCEDURE

The theoretical performance of LPD antennas is predicted in this paper using the type of analysis introduced by Carrel [2], with the addition of resistive losses in order to calculate the efficiency. These losses are calculated from the lossless current distribution and the surface resistance of copper at the frequencies used. The pertinent aspects of this formulation are as follows. The element feed-point voltages and currents are found from

$$[I_A] = \{[Y_F][Z_A] + [U]\}^{-1}[I] \quad (1)$$

where

$[I_A]$ element feed-point currents (N -row column matrix) where N is the number of elements in the antenna

Manuscript received May 19, 1969; revised September 11, 1969. This work was supported by the National Research Council of Canada under Grant A-4140.

The authors are with the Department of Electrical Engineering, University of Toronto, Toronto, Ont., Canada.

[I] driving current (N -row column matrix) where

$$I_n = 0, \quad n \neq N \\ = 1 + j0, \quad n = N$$

[Y_F] feeder admittance matrix ($N \times N$)

[Z_A] element impedance matrix ($N \times N$)

[U] unit diagonal matrix ($N \times N$).

The details of the matrices are given by Carrel [2]. Also

$$[V_A] = [Z_A][I_A] \quad (2)$$

where

[V_A] element feed-point voltages.

The input power to the antenna (fed by $1 + j0$ amperes at the N th element as shown in Fig. 1) is

$$W_{in} = \frac{1}{2} \text{Re} \{V_{AN}\} \text{ watts} \quad (3)$$

and the power lost in the elements is (for copper)

$$W_{loss} = (2.077 \times 10^{-8}) (f)^{1/2} \\ \cdot \sum_{i=1}^N |I_{A_i}|^2 (h_i/r_i) \left[1 - \frac{\sin 2\beta_0 h_i}{2\beta_0 h_i} \right] \text{ watts} \quad (4)$$

where

- β_0 free-space propagation constant
- h_i, r_i as in Fig. 1
- f frequency, hertz
- N number of elements.

The radiation patterns are given by

$$|E| = \left| \sum_{i=1}^N I_{A_i} (\sin \theta / \sin \beta_0 h_i) \exp [-j\beta_0 |x_i| \sin \theta \cos \phi] \right. \\ \left. \cdot [\cos (\beta_0 h_i \cos \theta) - \cos \beta_0 h_i] \right| \quad (5)$$

where

- I_{A_i} feed current in i th element
- x_i, h_i as in Fig. 1
- θ, ϕ spherical coordinate angles.

$\theta = \pi/2$ gives the H -plane pattern and $\phi = 0$ gives the E -plane pattern (Fig. 1). The efficiency η is defined as the ratio of power radiated to total power input or (in decibels)

$$\eta = 10 \log_{10} \left\{ \frac{W_{in}}{W_{in} + W_{loss}} \right\} = G - D \quad (6)$$

where G and D are the power gain and directivity (in decibels) defined later. Also, for the purposes of analysis, it is convenient to define

$$\eta' = G - D_{HP} \quad (7)$$

where D_{HP} is the half-power point directivity. Also

$$G = 10 \log_{10} \left\{ (60/W_{in}) \left| \sum_{i=1}^N I_{A_i} \exp [-j\beta_0 |x_i|] \right. \right. \\ \left. \left. \cdot (1 - \cos \beta_0 h_i) (1/\sin \beta_0 h_i) \right|^2 \right\} \quad (8)$$

$$D = 10 \log_{10} \{P_{max} 4\pi / W_{in}\} \quad (9)$$

where

P_{max} power density per unit solid angle in the direction of the maximum of the main beam

$$D_{HP} = 10 \log_{10} \{41 253 / \theta_H \theta_E\} \quad (10)$$

and where $\theta_H, \theta_E = H$ - and E -plane half-power beamwidths (in degrees). η' can be regarded as an approximate measure of efficiency, which is easily obtained experimentally and which can be compared to a calculated value. η' will differ from η only by the amount that D_{HP} differs from D (the former does not take back lobes into account), and its use avoids the difficulties inherent in obtaining a precise value for the directivity. Equation (10) could be revised to include the back lobe (approximating it in a manner similar to the main lobe), and would provide more meaningful directivity measurements over a larger range of parameters. The form used here, however, is suitable for a comparison between a measured and a calculated value.

The parameters of the LPD antennas studied experimentally and theoretically are shown in Fig. 1. They are at the intersection of seven constant- τ lines and ten constant- α lines (labeled A to G and 1 to 10, respectively). The eight values of α at $\tau = 0.962$ ($A1$ to $A8$) and the ten values of α at $\tau = 0.892$ ($D1$ to $D10$) were studied experimentally and all the values studied theoretically. A structure bandwidth of 2:1 (500–1000 MHz) was used to avoid excessive feeder lengths in large- τ models. An average length-to-diameter ratio of 145 was attained using copper rods and the feeder was spaced to give an unloaded impedance of 100 ohms. The feeder was made from solid copper-sheathed coaxial cables, balanced by connecting the center wire of one across to the outer sheath of the other at the feed point. The elements were soldered to the feeder and bent to lie coplanar, a necessity for meaningful comparison with theory in models with closely spaced elements. All models were terminated with a short circuit on the feed line at a distance $\frac{1}{8}$ of the resonant wavelength of the longest element behind this element ($s = h_1/2$ in Fig. 1).

An anechoic chamber, designed for use at or above 500 MHz was used for all measurements. Power gain measurements were made using a calibrated attenuator (relative accuracy of ± 0.1 dB) and comparison with a half-wavelength dipole. The input impedance and relative levels of back lobe and main lobe were measured with a swept-frequency system using a network analyzer.

RESULTS

Properties of Individual Antennas Over Operating Bandwidth

The measured variations in radiation patterns and input impedances for typical compressed and uncompressed LPD antennas are shown in Figs. 2 and 3. It can be seen from these figures that the variations over the operating bandwidth are about the same for compressed and uncompressed models, despite the fact that the actual patterns and input impedances are different in the two cases (the variations in input impedance refer to deviations from the average circle of impedance over one log period). This indicates that frequency-independent performance is retained by highly compressed LPD antennas. This may be better seen by considering the upper and lower band-limit frequencies shown in Fig. 4. They were determined by two criteria: the limits of the operating bandwidth were con-

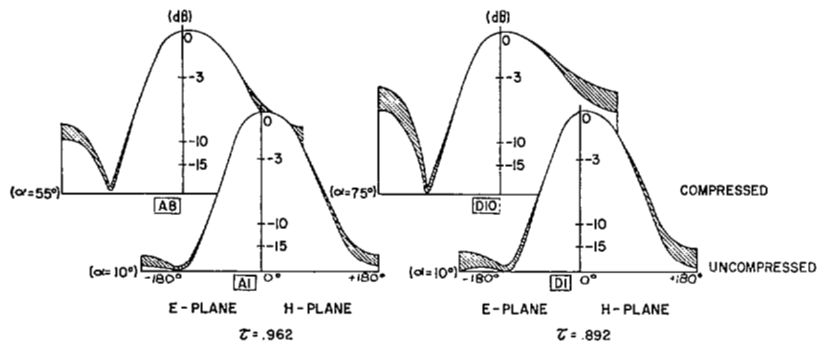


Fig. 2. Measured radiation pattern variation over operating bandwidth.

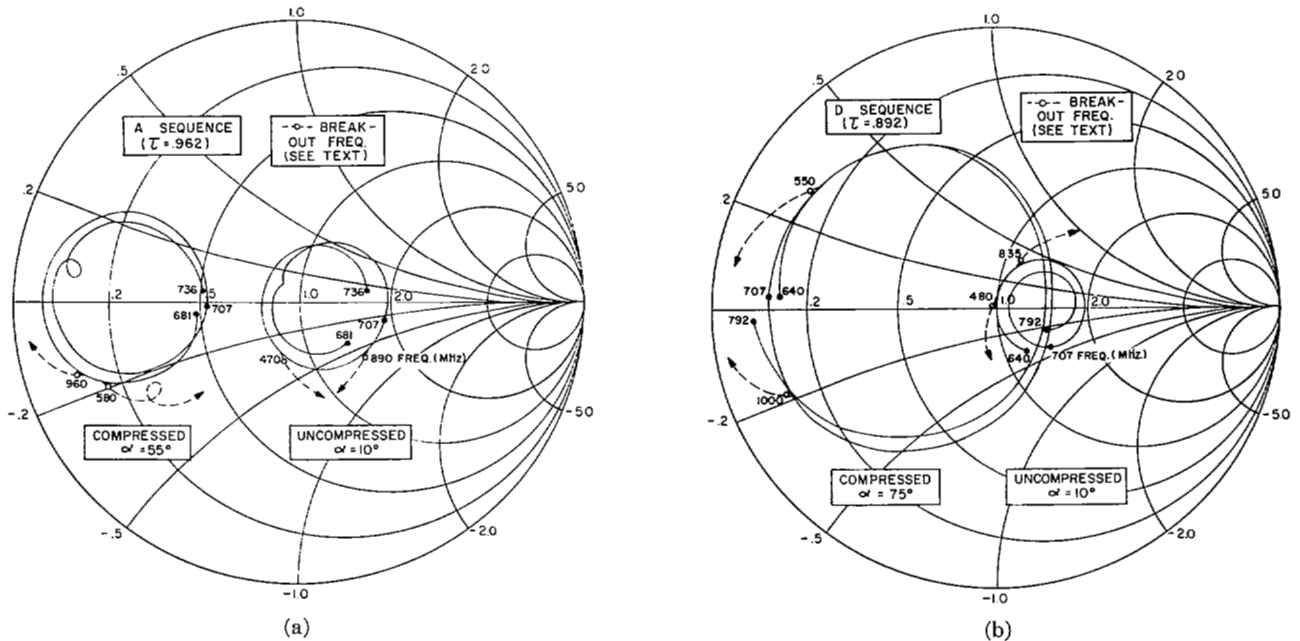


Fig. 3. Measured input impedance variation over center log periods (50-ohm impedance coordinates).

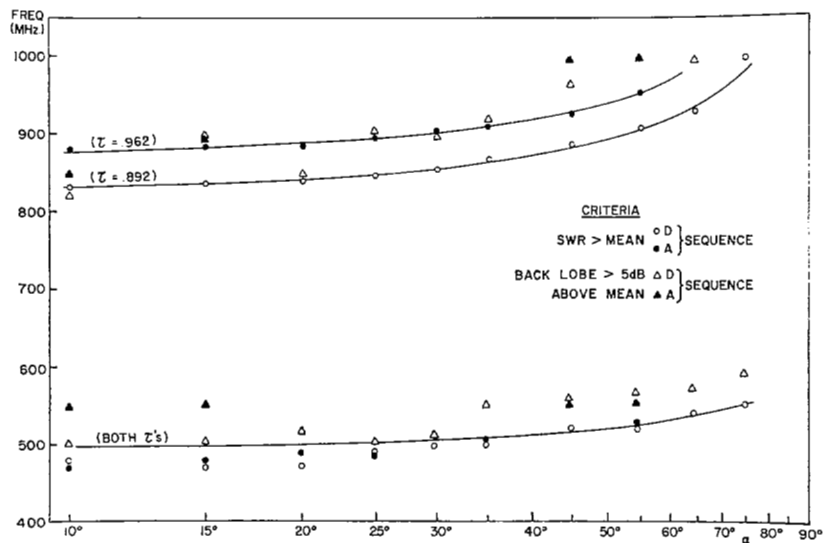


Fig. 4. Measured operating bandwidth for 2:1 structure bandwidth (indicated by upper and lower band-limit frequencies).

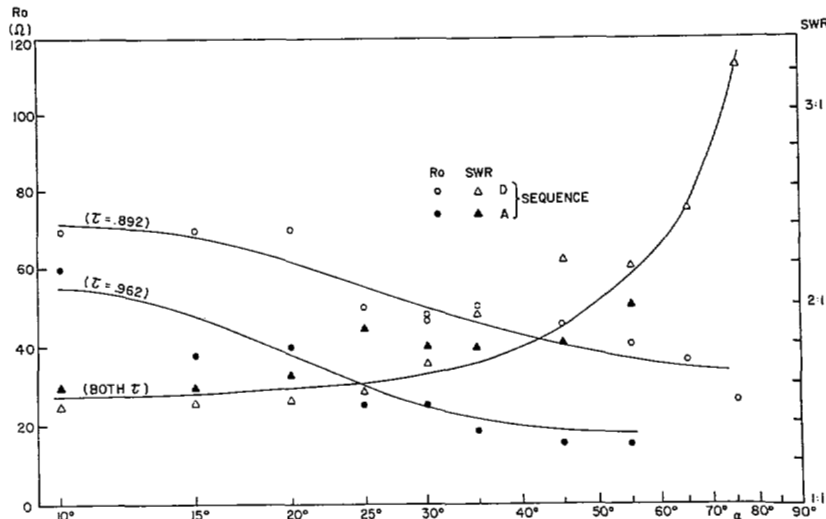


Fig. 5. Measured mean input resistance R_0 and SWR.

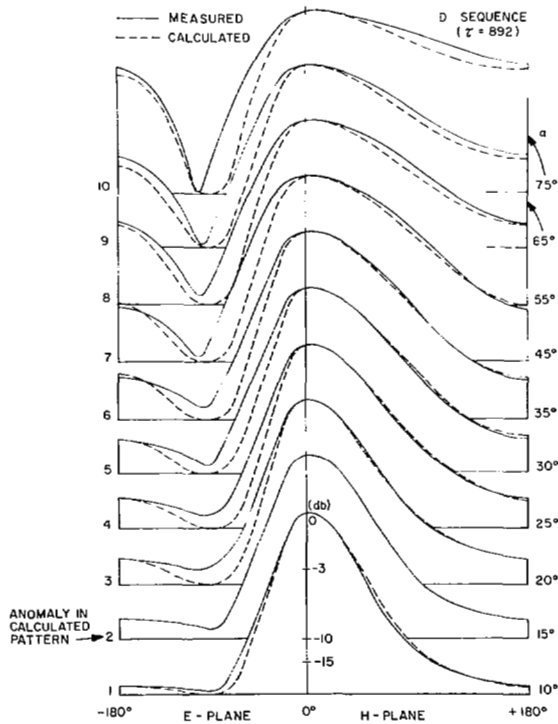


Fig. 6. Radiation pattern progression at 707 MHz.

considered reached when 1) the input impedance was observed to "break-away" from the well-defined circles displayed over the center range of frequencies and thus the standing-wave ratio (SWR) became greater than the mean midband value (these frequencies are shown by open circles and dashed lines in Fig. 3); and when 2) the back-lobe level rose to more than 5 dB over the mean midband value. The impedance criterion gave sharply defined upper and lower band-limit frequencies but the back-lobe criterion was more difficult to apply, especially when the midband back lobe was already quite high. Fig. 4 shows that the upper band-limit curve for models with large τ (many elements) lies entirely above that for models with lower τ (fewer ele-

ments). Evidently, the active region on antennas with a large τ consists of a sufficient number of elements (four or five) to allow it to move partially off the high-frequency end of the antenna without disrupting the normal midband characteristics. This is not the case, however, with smaller τ models where the active region contains only two or three elements. It is also interesting to note the effect of truncating the antenna at the high-frequency end. The electrical length of the truncated portion decreases as α increases, allowing better high-frequency performance (as can be seen in Fig. 4) and also allowing the impedance to return to a more constant value each log period [which can be clearly seen in Fig. 3(a)].

The mean input resistance R_0 and input SWR, as defined by Carrel, were found from results such as Fig. 3 and are shown in Fig. 5. It can be seen that R_0 decreases with increasing α and also as the number of elements increases. The SWR likewise increases with α , slowly at first and then very rapidly.

Highly compressed models (A8 and D10) are very sensitive to mechanical vibrations. The input impedance blossoms out and returns to normal in an oscillatory fashion when the antenna is subjected to even a slight mechanical shock.

Properties of Sequences of Antennas at Constant Midband Frequency

The effects of compressing a LPD antenna can be conveniently studied by examining the properties at a constant midband frequency. The calculated and measured progressions of radiation patterns and input impedances are shown in Figs. 6 and 7 for the two constant- τ sequences studied experimentally. The general trend in radiation patterns is toward dipole-like behavior as α approaches 90°, indicated by the rise in back-lobe level and by the H -plane patterns becoming more nearly constant. The input impedance tends to spiral outward in a counterclockwise direction toward lower values of R as α increases.

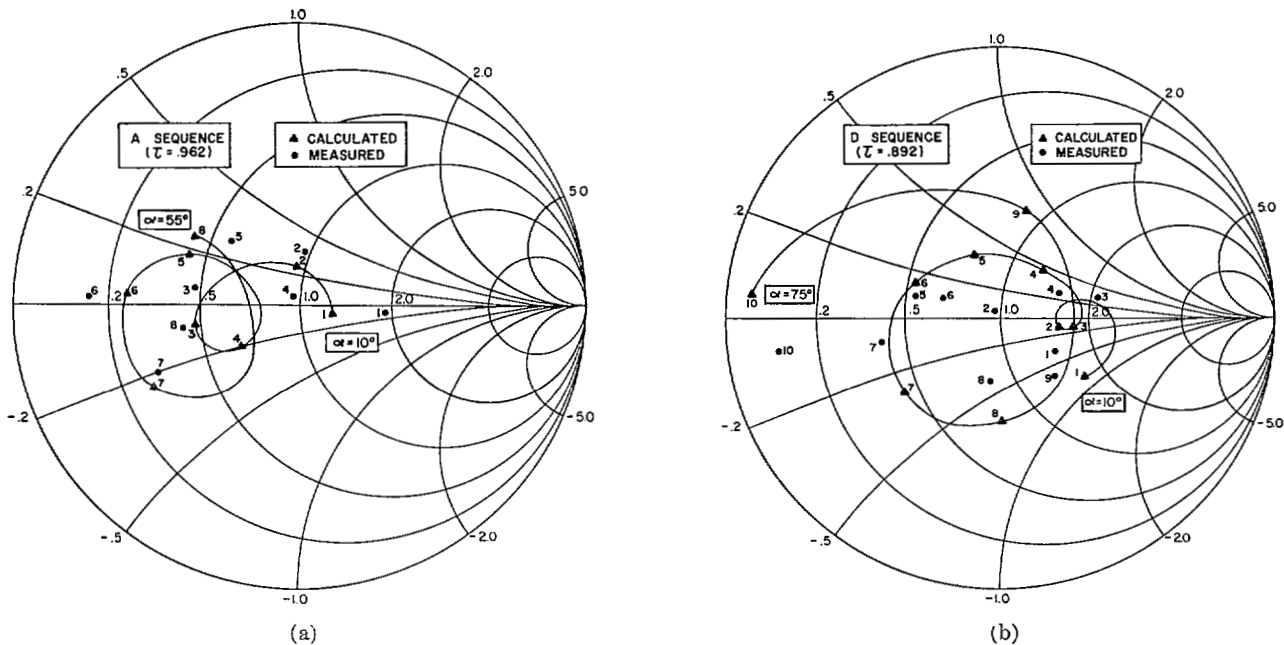


Fig. 7. Input impedance progression at 707 MHz; 50-ohm impedance coordinates; numbers refer to values of α shown in Fig. 1.

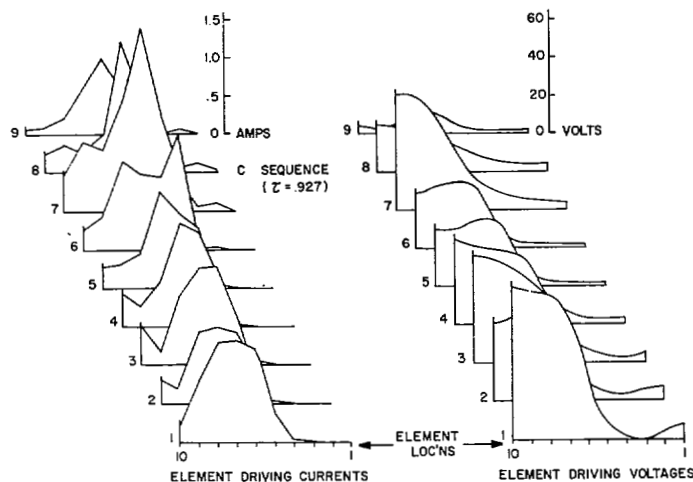


Fig. 8. Calculated progression of feeder characteristics at 707 MHz.

These trends are found to be common to all the constant- τ sequences studied theoretically. The experimental values shown in Figs. 6 and 7 agree well with those calculated with the exception of the widths of the E -plane main lobe, which are consistently wider than predicted. This suggests that the sinusoidal current distribution chosen for the elements is not entirely accurate. An analysis of a LPD antenna has been done by Cheong and King [6] using a more accurate current distribution.

The calculated progression of feeder characteristics is shown in Fig. 8. From this figure it can be seen that a well-defined active region remains on the antenna as it is compressed. This is characterized by a peak in the element driving currents and a drop in the element driving voltages. The existence of a well-defined active region is, of course, necessary for maintaining frequency independence as α

increases. It can also be seen from this figure that the active region becomes confined essentially to one element as α becomes large. If only one element is contributing significantly to the far-field radiation then one would expect dipole-like behavior.

The behavior of the power gain G , directivity D_{HP} , approximate efficiency η' , and true efficiency η as α increases is shown in Figs. 9 and 10. Both the gain and directivity decrease as α increases, the power gain at a faster rate since the back lobe is not considered in the directivity formula. The experimental values of power gain and directivity are consistently $\frac{1}{2}$ -2 dB below those calculated.

The experimental values of η' shown in Fig. 12 agree at least in trend with those calculated. Although the system error in measuring a value for η' (about ± 1 dB) precludes

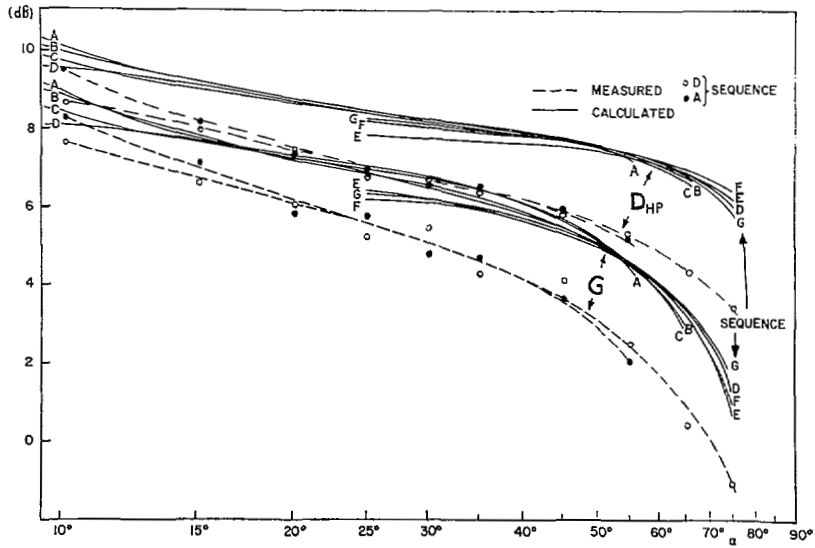


Fig. 9. Power gain and directivity at 707 MHz, relative to isotropic.

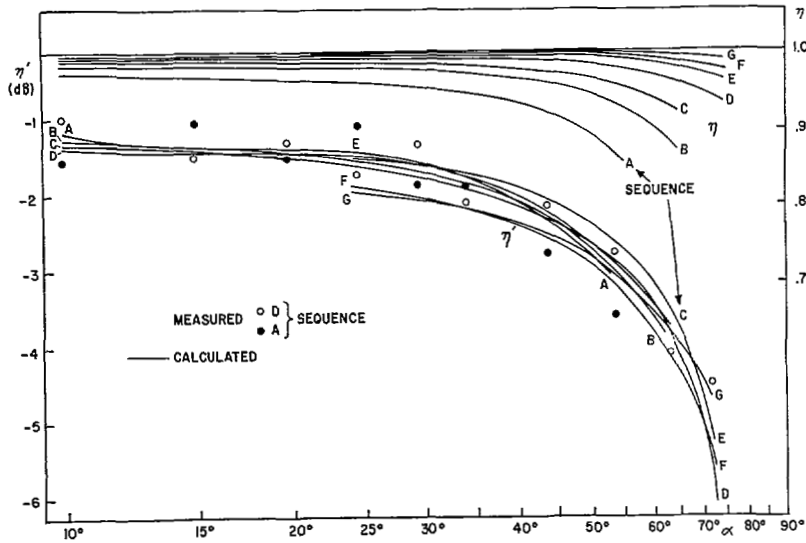


Fig. 10. Power gain minus directivity and calculated efficiency at 707 MHz.

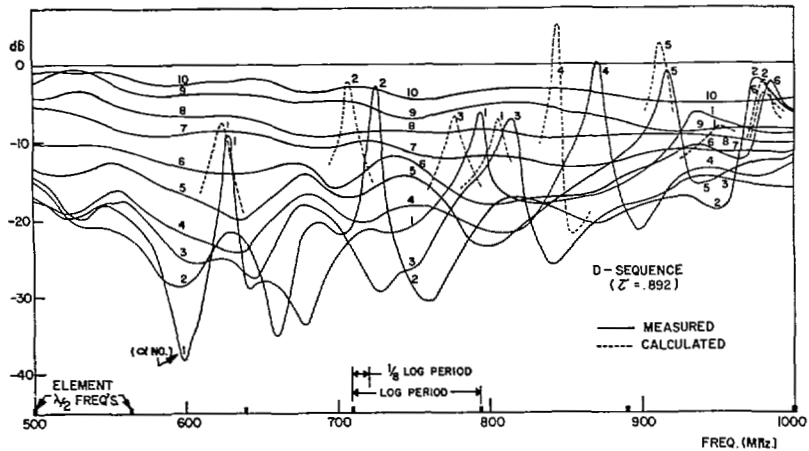


Fig. 11. Back-lobe levels, with respect to front lobe.

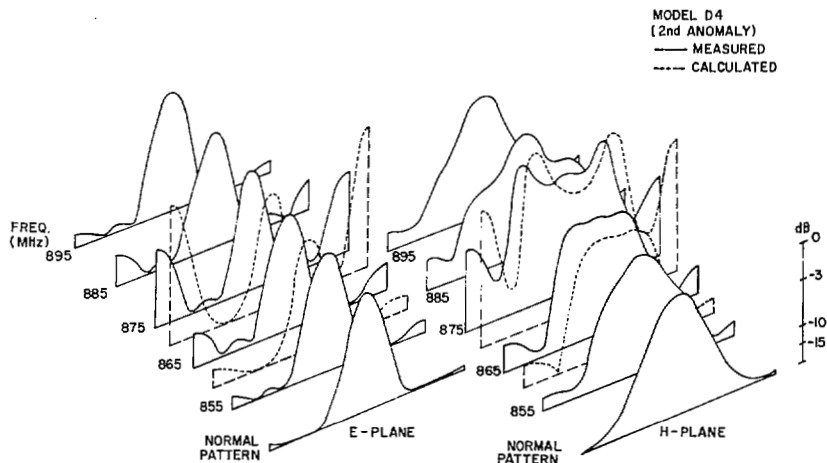


Fig. 12. Typical radiation pattern behavior through anomaly.

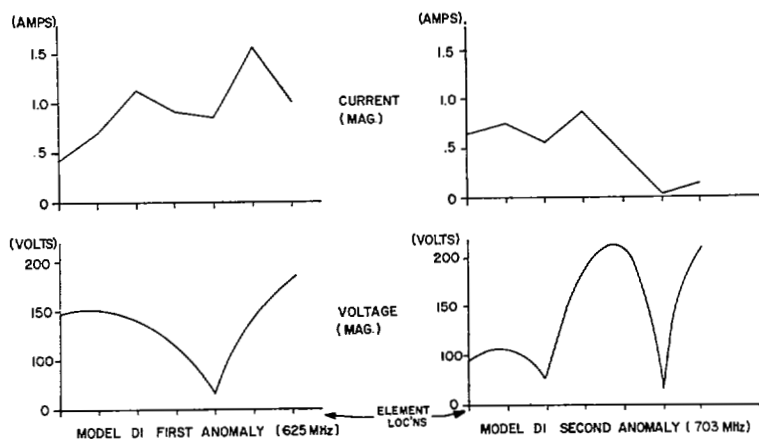


Fig. 13. Calculated anomalous feeder voltages and element driving currents.

any attempt to draw precise conclusions, the agreement is sufficiently good to suggest that the calculated values of η shown in Fig. 10 are representative of the actual efficiencies of the LPD antennas used experimentally.

Anomalous Frequency-Dependent Behavior

For the D sequence (models with seven elements), Fig. 11 shows swept-frequency measurements of the back-lobe level with respect to the main lobe. Prominently displayed in the figure are sharply defined peaks with widths of about $\frac{1}{8}$ of a log period. These peaks recur in a seemingly progressive and orderly fashion as α increases. The calculated back-lobe levels in Fig. 11 show good correspondence to the experimental values. Note that three such peaks occur on model D1, two on model D2, and none on models above D6. No such peaks occurred on A-sequence (19-element) models. Through these anomalies, the radiation patterns and feeder current and voltage distributions show marked changes from the normal midband properties, and the input impedances show slight to severe departures from the normal midband values. Examples of typical measured and calculated radiation patterns through an anomaly, shown in Fig. 12, display high sidelobes in the *H*-plane pattern (as well as the large back lobe) and a slight narrowing of the beamwidth in the *E* plane. Typical calcu-

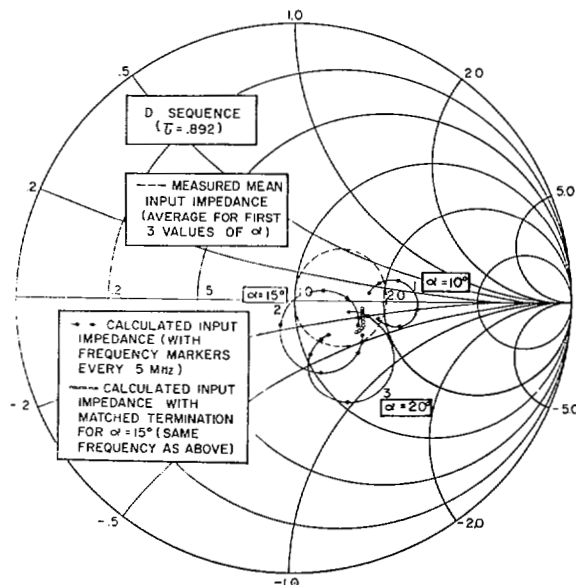


Fig. 14. Calculated input impedance behavior through anomalies, 50-ohm impedance coordinates.

lated feeder characteristics, shown in Fig. 13, display a splitting of the active region in the element driving currents and a marked standing-wave appearance in the voltage distribution. Fig. 14 shows how the calculated input im-

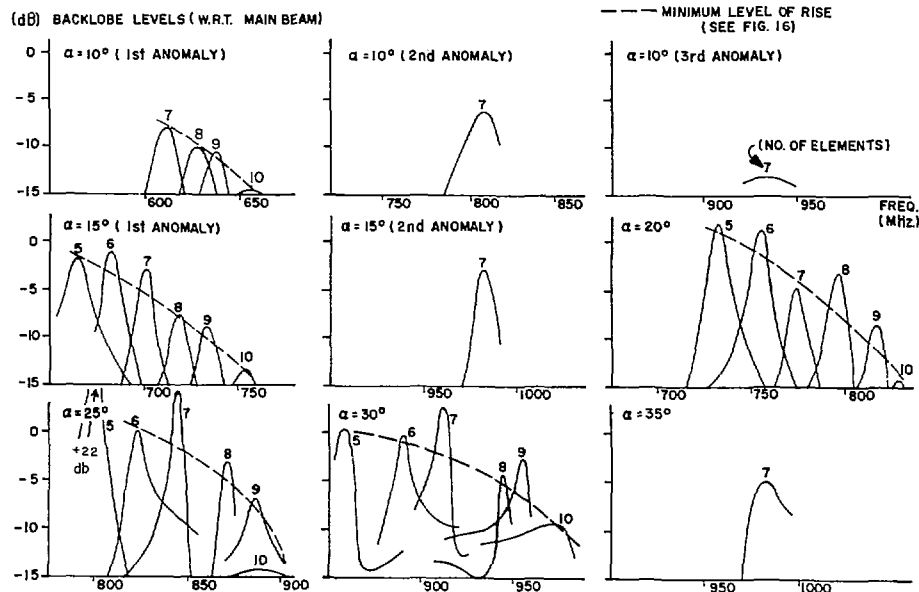


Fig. 15. Back-lobe levels through anomalies.

pedance behaves through an anomaly for the first three values of α . The main feature, typical of an anomaly, is a fast sweep through a (generally) reactive area. The 5-MHz spaced markers (dots) show how the input impedance changes rapidly through an anomaly and the dashed circle, which represents the measured mean input impedance under normal conditions (it is almost identical in extent for the first three values of α), shows how the impedance deviates from the normal through an anomaly. The calculated results for a matched termination are also shown.

The addition of three elements to the small end of the antenna has no effect on the anomalous behavior, whereas the addition of three elements to the large end restores normal behavior. Rather than remove the anomaly, however, the latter procedure merely moves it to another frequency. This indicates that the anomaly is caused by something at the large end of the antenna and furthermore that the effect is not due to the large elements behind the active region. This leaves reflections from the short-circuit termination as the cause of the anomalies. When a matched termination is used, no anomalous effects at all are noted. The open circles in Fig. 14 show that there is no unusual behavior in the input impedance for this case. Further analysis reveals that the location of the active region (or where it should be) at the peak of an anomaly falls just in front of a point $\lambda/2$ down from the short circuit (λ being the free-space wavelength). For model D1, the peaks correspond to the $\lambda/2$, λ , and $3\lambda/2$ points; for D2 they correspond to the $\lambda/2$ and λ points; and for models above D6 the feeder was too short for even the $\lambda/2$ point. Thus it would appear that inefficient coupling to the elements causes sufficient power to remain on the feeder past the active region to produce reflections from the short circuit that subsequently disrupt the active region and prevent the normal operation of the antenna. This disruption seems to occur only when the location of the active region is at an $n\lambda/2$ point or null point in the standing-wave pattern set up in the voltage distribution.

An extensive computer analysis was made to determine what number of elements in a 2:1 bandwidth (i.e., τ) was sufficient to have a noticeable effect on the back-lobe level. The results are displayed in Fig. 15. They clearly show that the effect of the anomaly gets worse (i.e., the rise in back-lobe level increases) as the number of elements decreases. Also the effect is barely noticeable for more than ten elements. Notice that the anomaly occurs at slightly different frequencies for different numbers of elements for a constant α . Also the effect of an anomaly on the input impedance is to make the fast sweeps into the reactive region progressively more extensive.

These results can be conveniently displayed in the form of back-lobe-level contours on a τ - σ diagram, as shown in Fig. 16. These contours represent the minimum level to which the back lobe can be expected to rise (dashed lines in Fig. 15) with respect to the main beam, at the peak of an anomaly. Note that these represent a minimum level of back-lobe rise (in model E4 for example the back lobe rose to +22 dB above the front lobe). From Fig. 16 it would appear that an element density of at least ten elements per 2:1 bandwidth ($\tau \approx 0.925$) is required before the backlobe remains at least 15 dB below the main beam through an anomaly.

Carrel [2, pp. 77 and 91] mentions that when a reactive termination is used for an eight-element LPD antenna with $\tau = 0.888$ and $\sigma = 0.089$, the input impedance locus over a few log periods blossoms out with respect to the impedance for a matched termination, indicating that end effects are appreciable. He also mentions that irregularities in the pattern occur, although he does not explain what they are. In order to investigate the problem of power remaining on the transmission line past the active region, Carrel [2, p. 74], defines an efficiency (which we shall call η'' here) as the ratio of power input minus the power lost in a matched termination to power input. For a feeder impedance of 100 ohms the results he obtains indicate that more than 10 percent of the input power is lost in the

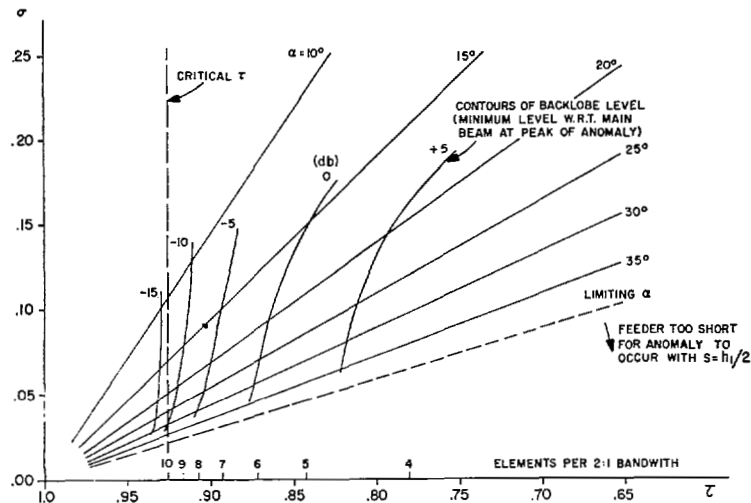


Fig. 16. Minimum peak back-lobe levels through anomaly, with respect to front lobe.

termination when τ is less than about 0.85. He summarizes by stating that for a feeder impedance allowing a value of η'' to be greater than 0.9, a short-circuit termination $\lambda_1/8$ behind the largest element is satisfactory for the range of parameters $0.8 < \tau < 0.98$ and $0.03 < \sigma < 0.23$. However, it would appear from the results presented here that, even in the range of parameters cited by Carrel, satisfactory operation is not always achieved using a short-circuit termination. Theoretical calculations show that the amount of reflected power is small. For instance, when the short-circuit termination of model D2 was replaced by a matched load at the frequency corresponding to the peak of the first (703 MHz) anomaly, only $2\frac{1}{2}$ percent of the input power was absorbed by the load. Apparently, this small amount of power remaining on the transmission line past the active region was sufficient to cause the anomaly.

CONCLUSIONS

It has been shown that a compressed LPD antenna retains frequency independence up to and beyond the point where the actual properties become undesirable for most applications. The overall effects of compression are a rise in the back-lobe level, a lowering of the mean input resistance and gain, and an increase in input SWR. These effects are small for α less than about 45° and become marked for larger α . Highly compressed models exhibit a marked sensitivity to mechanical vibration.

It has also been shown that when a reactive termination is used for a LPD antenna there is a lower limit on τ of about 0.92–0.93 if anomalous behavior is to be avoided.

This anomalous behavior results in severe pattern lobing over narrow frequency bands with widths of about $\frac{1}{3}$ of a log period. The lower limit on τ is equivalent to a lower limit on the element density of about ten elements per 2:1 bandwidth. Anomalous behavior was found to exist on all models of suitable τ regardless of σ or α except when the total feeder length is less than half of the shortest wavelength used. All anomalous behavior can be avoided if a matched termination is used and the losses in such a termination will be small. This can, however, create problems in supporting the antenna. Therefore in most practical situations one is obliged to use a short-circuit termination. If the antenna has a τ less than 0.92 the problem of anomalous behavior can be minimized by a judicious choice of location for the termination, to place as few as possible of the voltage null points on the feeder.

REFERENCES

- [1] D. E. Isbell, "Log periodic dipole arrays," *IRE Trans. Antennas and Propagation*, vol. AP-8, pp. 260–267, May 1960.
- [2] R. L. Carrel, "Analysis and design of the log-periodic dipole antenna," Antenna Lab., University of Illinois, Urbana, Tech. Rept. 52, 1961.
- [3] D. T. Stephenson and P. E. Mayes, "Broadband arrays of helical dipoles," Antenna Lab., University of Illinois, Urbana, Tech. Rept. 2, Contract NEL 30508A, 1964.
- [4] J. S. Chatterjee and M. N. Roy, "Helical log-periodic array," *IEEE Trans. Antennas and Propagation* (Communications), vol. AP-16, pp. 592–593, September 1968.
- [5] D. F. DiFonzo, "Reduced size log-periodic dipole antennas," *Microwave J.*, vol. 7, pp. 37–43, December 1964.
- [6] W. M. Cheong and R. W. P. King, "Log-periodic dipole antenna," *Rad. Sci.*, vol. 2, pp. 1315–1325, November 1967.
- [7] P. G. Ingerson and P. E. Mayes, "Log-periodic antennas with modulated impedance feeders," *IEEE Trans. Antennas and Propagation*, vol. AP-16, pp. 633–642, November 1968.